DRAG REDUCTION BY DIMPLES? – A COMPLEMENTARY EXPERIMENTAL/NUMERICAL INVESTIGATION –

Hermann Lienhart, Michael Breuer, Cagatay Köksoy
Institute of Fluid Mechanics
University of Erlangen–Nürnberg
Cauerstr. 4, D-91058 Erlangen, Germany
lienhart / breuer / ckoeksoy @lstm.uni-erlangen.de

ABSTRACT

The paper is concerned with experimental and numerical investigations on the turbulent flow over dimpled surfaces. Shallow dimples distributed regularly over the wall of a plane channel with large aspect ratio are used to study their effect on the friction drag. The resulting pressure drop in the channel was measured for smooth and dimpled walls. In addition to these investigations on internal flows, an external flow study was performed and boundary layer profiles were measured using a Pitot tube rake. Complementary to the measurements, direct numerical simulations for the internal flow configuration with and without dimples were carried out for two different grid resolutions and analyzed in detail. The objective is to clarify and prove or disprove the effect of dimples on the skin friction drag.

INTRODUCTION

A regular arrangement of troughs called *dimples* is a well-known measure to increase heat transfer from a wall. Compared to a smooth wall, the Nusselt number can be significantly enhanced by dimples, whereas the increase of the pressure drop was found to be small. For that purpose, deep dimples with a ratio of depth to print diameter of $h/D = 0.2 - 0.5$ are typically applied which enhance the convective transport from the wall (see e.g. Burgess et al. (2003)).

Some years back Russian scientists (see, e.g., Alekseev et al. (1998)) found out that apart from heat transfer enhancement dimples might be useful for drag reduction. Their findings are based on experimental measurements of turbulent flows over surfaces with a regular arrangement of *shallow* dimples leading to a decrease of the skin friction drag of a turbulent flow up to 20% (no golf ball effect!). However, up to now no clear explanation was provided which can illuminate this effect. Hence some doubts remain regarding the experimental investigations and their outcome. Compared to classical devices for drag reduction such as riblets, shallow dimples would be advantageous since they are composed of macroscopic structures which are less sensitive to dirt and mechanical degradation. Furthermore, they do not depend on the flow direction.

Since the drag reduction promised by dimples would have a tremendous economical influence, it is worth to study it in more detail. For that purpose, experimental investigations as well as direct numerical simulations (DNS) of the turbulent flow inside a channel with dimpled walls were carried out to investigate the physical mechanism. As the reference test case the fully developed turbulent channel flow was chosen because it offers several significant advantages: there are no other drag components involved but skin friction, the boundary conditions are very well defined and the wall shear stress can be deduced from relatively simple and reliable pressure drop measurements. In order to verify the findings of the internal flow tests, some complementary measurements in a zero gradient boundary layer were added. For this test case a Pitot tube rake was adopted as the measuring technique.

EXPERIMENTAL SET-UP

Internal Flow

The experimental investigation for internal flows was performed in the channel test rig sketched in Fig. 1. It consisted of the blower / settling chamber unit, the channel test section with exchangeable walls and the measuring instrumentation. The air flow was provided by a centrifugal blower, the flow rate was varied by means of a closed loop rpm control unit. The settling chamber was equipped with honeycomb flow straightener and screens, thus ensuring well controlled flow conditions. The dimensions of the test section (50 mm $\times$ 600 mm $\times$ 6000 mm) were chosen in such a way that two-dimensionality and fully developed state of the channel flow was assured: the aspect ratio of the channel was set to 12, the length over height ratio to 120. In order to accelerate the evolution to the fully developed state a trip was introduced at the channel inlet. The walls of the channel were constructed from aluminum or poly-acrylic plates, respectively. The dimples of depth $h = 0.75$ mm and print diameter $D = 15$ mm were milled by a numerically controlled machine and polished (see Fig. 2). They are arranged regularly on one channel wall as will be shown below.

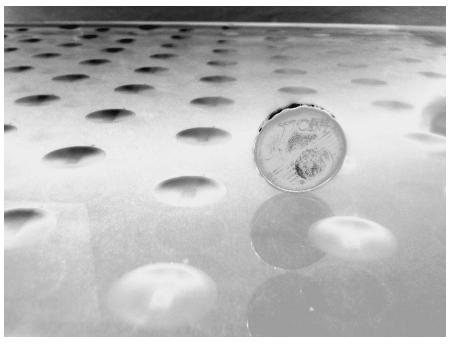

Figure 2: Plate with milled dimples.

The flow rate, and thus the bulk velocity, was measured using an inlet contraction in front of the blower. Density and viscosity of the air were derived from ambient pressure and temperature. The pressure instrumentation consisted of a Scanivalve unit and a Validyne differential pressure gauge. For each test Reynolds number the pressure gradient was deduced by a linear fit of the measured pressure data and

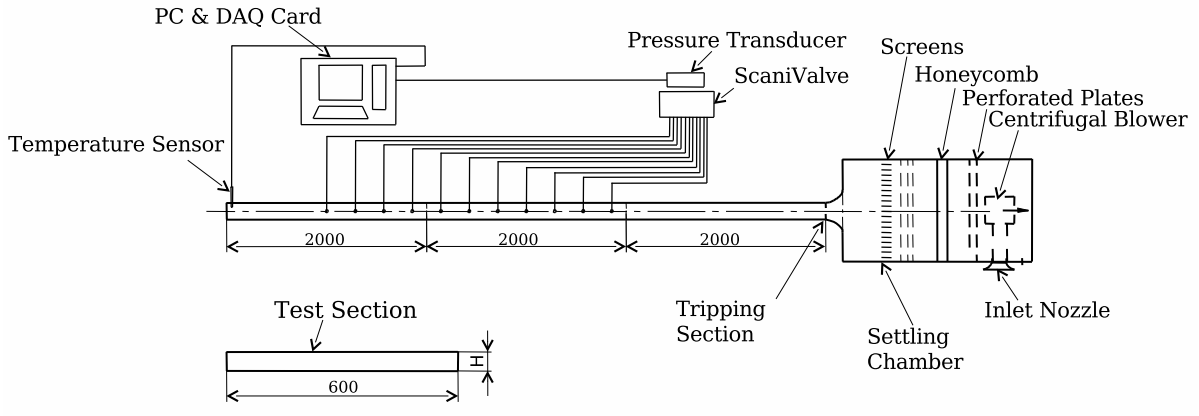

Figure 1: Experimental set-up of the plane channel flow.

the results reduced to wall shear stress and skin friction coefficient.

External Flow

The external flow study was performed in the open test section closed loop wind tunnel of LSTM Erlangen. The test section of the tunnel was 1.87 × 1.4 m^2 in cross-section and the turbulence level of the flow was less than 0.3%.

The test plate was mounted vertically in the test section of the wind tunnel and its orientation relative to the flow was adjusted so that the pressure taps that were placed at the locations A and B, as sketched in Fig. 3, read identical values. In this way it was ensured that zero pressure gradient was achieved along the plate surface. The width of the plate is wide enough, 1.24 m, to guarantee the three-dimensional flow at the edges of the plate not to propagate and disturb the boundary layer in the center plane of the plate, where the measurements were performed.

Boundary layer velocity profiles were measured using a Pitot tube rake, Fig. 4, which was constructed according to the recommendations given in Bui et al. (2000). The pressure readings of the rake were acquired by a Baratron Type 698A high accuracy pressure transducer and a 670B signal conditioner. Switching between the individual Pitot tubes was performed by means of a computer controlled Scanivalve.

The smooth plate measurements performed for comparison reasons were carried out by covering the dimpled plate with a 1 mm stainless steel sheet. Covering the plate instead of exchanging the dimpled plate by a smooth one eliminates any relative positioning errors and errors in pressure gradient, respectively.

The velocity profiles in the front and rear part of the test plate were measured at locations A and B. Based on this data the momentum loss of the test plates was calculated and the skin friction coefficients were deduced.

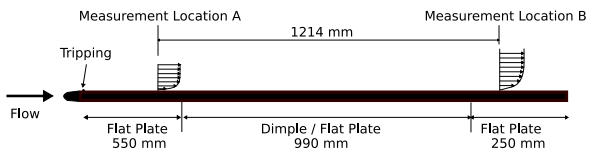

Figure 3: Experimental set-up of external flow measurements.

DIRECT NUMERICAL SIMULATIONS

Numerical Methodology

The direct numerical simulations were carried out with the CFD code $\mathcal{LESOCC}$ which was developed for the simulation of complex turbulent flows using either the methodology of DNS, large-eddy simulation (LES), or hybrid LES-RANS coupling. $\mathcal{LESOCC}$ is based on a 3-D finite-volume method for arbitrary non-orthogonal and non-staggered, block-structured grids (Breuer and Rodi, 1996; Breuer, 1998, 2002). The spatial discretization of all fluxes is based on central differences of second-order accuracy. A low-storage multi-stage Runge-Kutta method (second-order accurate) is applied for time-marching. In order to ensure the coupling of pressure and velocity fields on non-staggered grids, the momentum interpolation technique is used. $\mathcal{LESOCC}$ is highly vectorized (> 99.8%) and additionally parallelized by domain decomposition using MPI. The present simulations were carried out on the NEC SX-8 machine at HLRS Stuttgart using 8 processors of one node leading to a total performance of about 52.7 GFlop/s.

Description of the Configurations

In order to investigate the effect of dimples, a classical wall-bounded flow often studied in literature is considered, i.e., a turbulent plane channel flow at $Re = U_b\delta/\nu = 10,935$

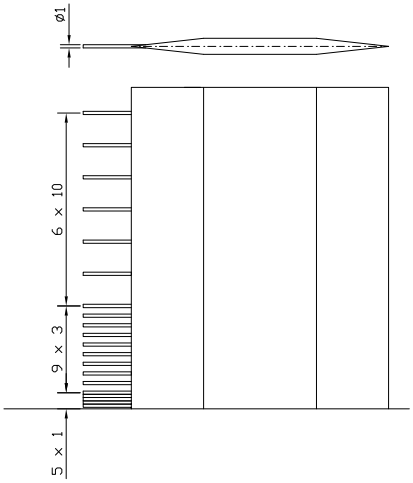

Figure 4: Sketch of the boundary layer rake used in the experiment.

or $Re_\tau = 590$. This test case has several advantages. With smooth non-dimpled walls the flow is homogeneous in streamwise and spanwise direction. That issue allows to apply periodic boundary conditions in both directions and thus avoids the definition of appropriate inflow and outflow boundary conditions. The pressure gradient in streamwise direction is adjusted such that a fixed mass flow rate ($U_b = const.$) is assured. Furthermore, no-slip boundary conditions are used at both walls.

Since the simulation cannot cover the entire experimental set-up, the computational domain consists of a cutout of the channel as sketched in Fig. 5 allowing to apply periodic boundary conditions in streamwise and spanwise direction. The extensions of the domain are $4.1744\,\delta \times 2\,\delta \times 2.4096\,\delta$, while all geometrical quantities are scaled by the channel half–width δ. Three cases are considered:

- **L**: Plane channel with multiple dimples at the **L**ower wall
- **B**: Plane channel with multiple dimples at **B**oth walls
- **R**: Plane channel without dimples, i.e., smooth walls as **R**eference case

As shown in Fig. 5 multiple shallow dimples (depth to print diameter of $h/D = 0.05$; $D/\delta = 0.6$) are arranged regularly on the surface of the lower and/or upper channel walls.

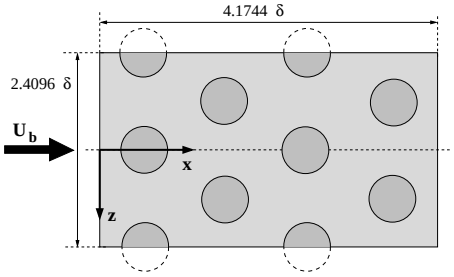

Figure 5: 2–D Sketch (**x**–**z**–plane) of the channel with multiple shallow dimples at the wall.

Using block-structured curvilinear grids, two different grid resolutions are taken into account for the DNS predictions, see Table 1. The first denoted *coarse grid* consists of about 5.5 million control volumes (CVs) and thus is not really coarse. For the plane channel case the grid is Cartesian with equidistant grid spacing in streamwise and spanwise directions and a stretched distribution towards both walls according to a geometric series. However, the expansion factor of the geometric series is mild ($r = 1.04$) and the first node is located at a dimensionless distance of $\Delta y^+_{min} = 0.587$. Hence several grid points are found in the viscous sublayer and the resolution in the homogeneous direction expressed in wall coordinates is of the order $\mathcal{O}(10)$. For the cases with dimples the grid is clinging to the curvilinear geometry of the walls and thus locally no longer Cartesian.

For the second grid denoted *fine grid*, the number of control volumes is exactly doubled in each direction for the computational domain sketched in Fig. 5, but due to some extra cells required for the periodic boundary conditions, the numbers given in Table 1 are not exactly doubled. In total about 43 million CVs are used and the resolution in each direction is halved as visible from the values for Δx^+, Δy^+_{min}, and Δz^+ summarized in Table 1. The dimensionless time step sizes are $\Delta t = 4.2 \times 10^{-3}$ and $\Delta t = 1.6 \times 10^{-3}$ for the coarse and fine grid, respectively. To achieve reliable statistical data, the flow is averaged over dimensionless time intervals of up to $T_{avg} = 1900$ and $17,000$ for the fine and the coarse grid, respectively, which is equivalent to about 450/4000 flow–through times.

Table 1: Overview on simulation parameters for the five simulations carried out.

Parameter	**Coarse Grid**	**Fine Grid**
Resolution (# CVs)	$260 \times 160 \times 132$	$516 \times 320 \times 260$
$\Delta y_{min}/\delta$	10^{-3}	5×10^{-4}
expansion ratio r	1.040	1.023
Δx^+	9.58	4.79
Δy^+_{min}	0.587	0.293
Δz^+	11.05	5.52
Δt	4.2×10^{-3}	1.6×10^{-3}
Cases considered	**L, B, R**	**B, R**

RESULTS

According to former studies the skin friction coefficients measured in the channel flow were plotted as a function of Reynolds number. Fig. 6 presents a summary of the experimental results together with data points derived from integration of the numerically obtained wall quantities. For comparison, data available in the literature (Dean, 1978) was added. The experimental skin friction coefficients for the channel flow with smooth walls and with a dimpled wall on one side almost collapse. They differ by less than 1% through all the Reynolds number range considered. Therefore, it may be concluded that, surprisingly enough, the dimpled wall did not show any increase in pressure loss, but a significant decrease could also not be detected.

This conclusion is also supported by the results of the measurements in the zero pressure gradient boundary layer of the external flow. Table 2 summarizes the differences in momentum loss over the smooth and the dimpled surface at two different flow velocities. The quantities displayed have to be considered to lie within the margins of the measurement uncertainties.

Table 2: Skin friction coefficients deduced from the external flow measurements.

U	**6 m/s**	**12 m/s**
$\frac{C_f^{dimple} - C_f^{smooth}}{C_f^{smooth}}$	-0.38%	2.02%

More insight into this not very satisfactory result regarding the integral behavior of the dimpled surface compared to the flat walls was tried to achieve using CFD. Since only minor deviations were found between the results obtained on the coarse and the fine grid, in the following only the latter are discussed.

First the quality of the results was checked by comparison of the present predictions with the well-knwon DNS data by Moser et al. (1999) for the plane channel flow. Exemplarily, Fig. 7 depicts the distribution of the mean velocity and the normal Reynolds stress $\overline{u'u'}$. For all quantities shown (and also those not shown here) an excellent agreement is found between the present DNS predictions and the literature data.

Figure 8 depicts results obtained for the case **B** using a regular arrangement of shallow dimples as shown in Fig. 5

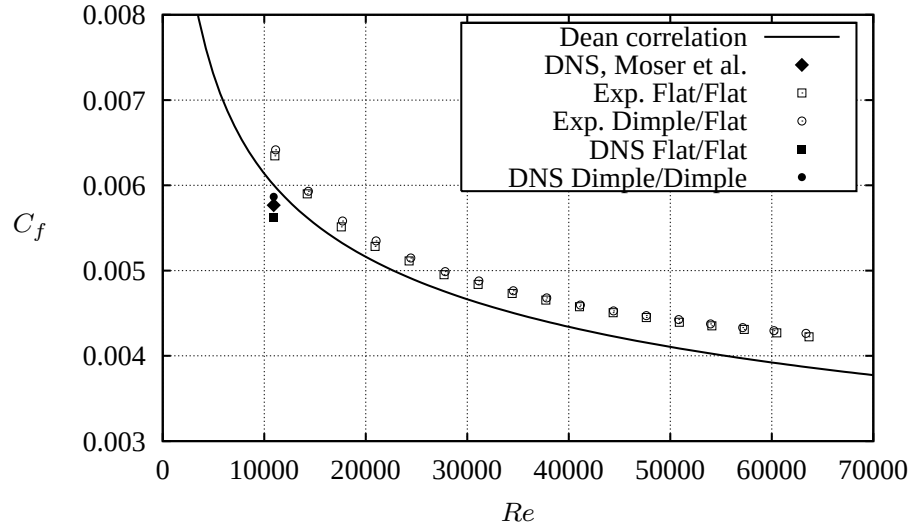

Figure 6: Measured and predicted friction coefficient C_f vs. Re for different configurations; reference data: Dean correlation (Dean, 1978) for smooth wall, $C_f = 0.06138 \times Re^{-1/4}$ and DNS by Moser et al. (1999).

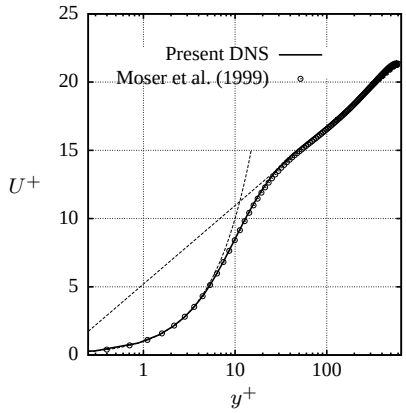

(a) **Mean Velocity**

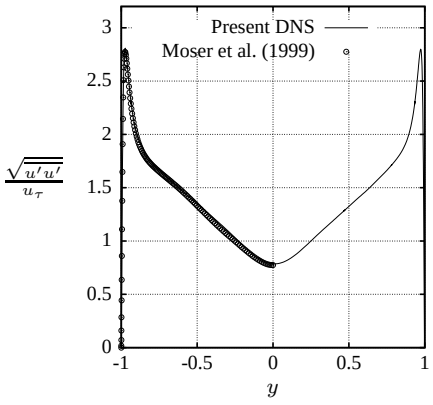

(b) **Normal Reynolds Stress** $\overline{u'u'}$

Figure 7: Channel flow without dimples, case **R**, $Re = 10,935$, comparison of present DNS predictions with DNS data by Moser et al. (1999).

at both walls. The time–averaged pressure distribution is shown in Fig. 8(a). The influence of the dimples on the pressure distribution at the lower wall can clearly be seen. It has to be mentioned here that the linear pressure gradient in the streamwise direction of the channel is not included in the figure. In Fig. 8(b) the time–averaged wall shear stress distribution is displayed. Obviously the wall shear stresses are decreasing within the dimples, leading to a very small recirculation region at the falling edge (see Fig. 9). However, at the border of the dimples where the fluid flow is leaving the troughs again, large values of the wall shear stress are found.

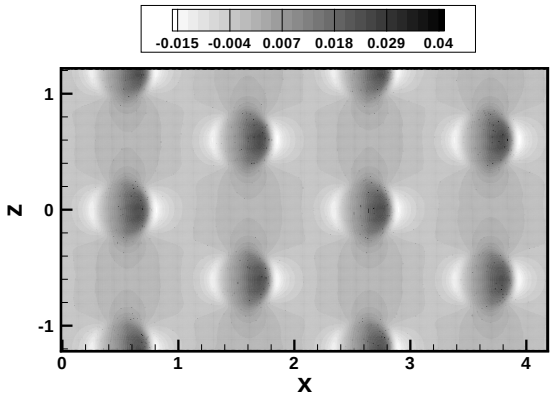

(a) **Time–averaged pressure**

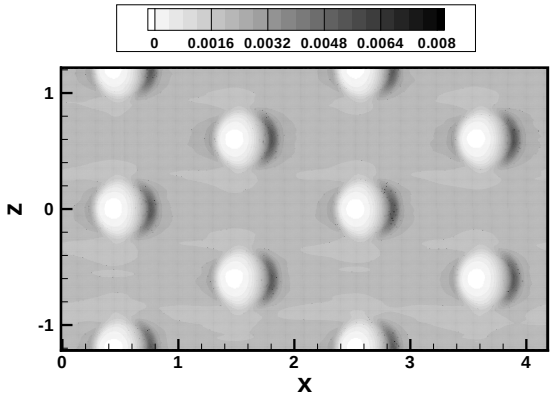

(b) **Time–averaged wall shear stress**

Figure 8: Channel flow with multiple dimples at both walls, case **B**, fine grid simulation, $Re = 10,935$.

In Fig. 9 the wall streamlines at the lower walls are dis-

played together with the distribution of the time–averaged spanwise ($\overline{w}$) and streamwise ($\overline{u}$) velocities close to the wall. In front of the dimple and partially also in the dimple the streamlines are converging. A tiny recirculation region with negative values of $\overline{u}$ visible in Fig. 9(b) is found inside the dimple. The existence of this phenomenon is confirmed by the results on both grids. At the side and past the recirculation region the streamlines are diverging again.

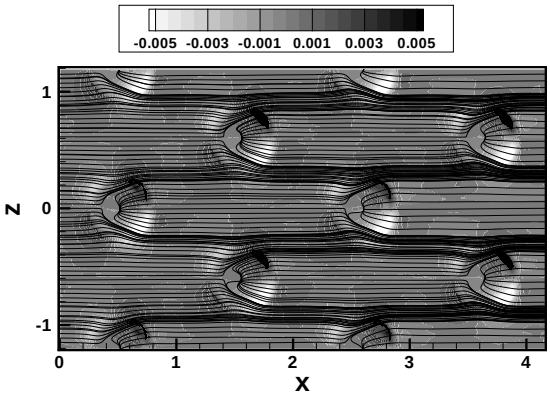

(a) **Wall streamlines / contours of $\overline{w}$ close to wall**

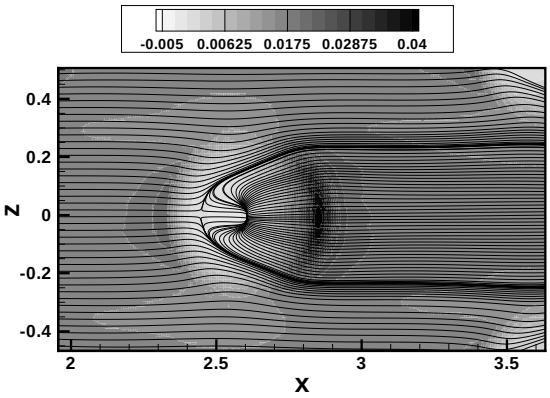

(b) **Zoom of wall streamlines / $\overline{u}$ close to wall**

Figure 9: Channel flow with multiple dimples at both walls, case **B**, fine grid simulation, $Re = 10,935$.

Figures 10(a)–(b) display the time–averaged flow in a x–y midplane of one dimple. Based on the velocity vectors the reduction of the velocity gradient near the wall and thus of the wall shear stress is visible. On the other hand, it is obvious that the structure of the wall leads to a modified pressure distribution compared with the case of a smooth wall. At both borders of the dimple when the flow is either entering or leaving the trough, the pressure is slightly decreasing. However, more important is the observation that the pressure is increasing on the rising edge of the dimple yielding a contribution to the overall drag resistance as will be shown below. The strongest flow structures in the time–averaged flow visualized by iso-surfaces of $\lambda_2 = -0.05$ are located at the borders of the dimple where the flow is entering or leaving the dimple.

Finally, Fig. 11 depicts time histories of the forces acting on the lower dimpled wall of case **B** and on the non–dimpled smooth wall of case **R**. For the non–dimpled wall the situation is simple since on this surface only the wall shear stress leads to a skin friction drag. This force (F_s) also acts on the lower dimpled wall where the time–average is marginally smaller on the dimpled wall than on the smooth wall (see also Table 3). However, at the dimpled wall the pressure

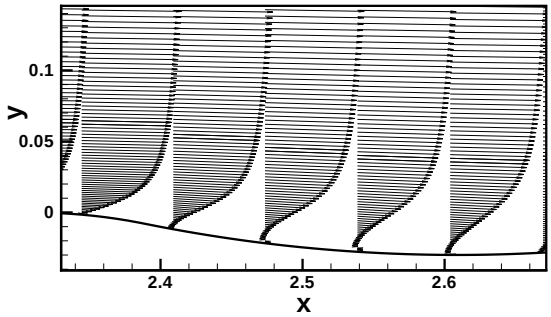

(a) **Zoom of the dimple region in a x–y midplane**

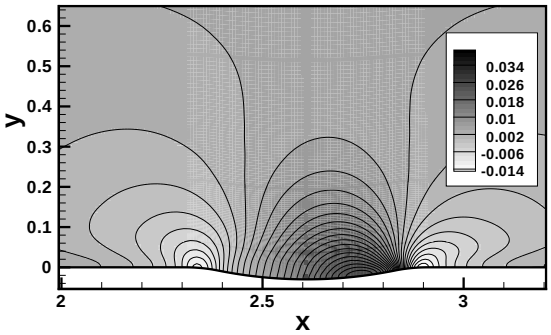

(b) **Contours of $\overline{p}$ in the dimple in a x–y midplane**

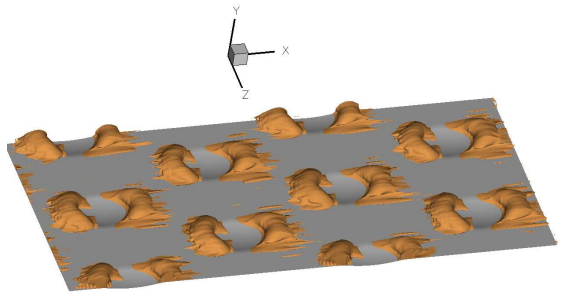

(c) **Iso-surfaces of $\lambda_2 = -0.05$**

Figure 10: Channel flow with multiple dimples at both walls, case **B**, fine grid simulation, $Re = 10,935$.

distribution on the wavy surface (Fig. 10(b)) yields a pressure force F_p in the main flow direction (about 5% of total force) which contributes to the total drag force F_t. Both effects, the slight decrease of the shear force F_s in average and the additional contribution of the pressure force F_p approximately compensate each other so that no net gain for drag reduction due to dimples remains. Presently, the total drag resistance for case **B** even increases about 4.4 % compared to the reference case **R** on the fine grid. For the coarse grid we found an increase of 1.9% or 3.8% for the case **L** with one dimpled wall and case **B** with two dimpled walls, respectively. Thus the effect of the dimples is doubled for case **B** compared with case **L** and an increase of about 4% is found for case **B** on both grids. Hence these simulations confirm the experimental findings that the present arrangement of dimples does not lead to drag reduction but even to a slight increase of the total drag.

CONCLUSIONS

Based on the simulations and the measurements described above, the question whether the present arrangement of dimples lead to drag reduction has to be answered with no.

Table 3: Integral results for all cases; $\overline{F}$ denotes the time–averaged forces on the lower and upper walls; indices p, s and t denote pressure, shear and total, respectively.

	Coarse Grid			Fine Grid	
	L	**B**	**R**	**B**	**R**
Lower Wall					
$\overline{F}_p$	.00152	.00153	0	.00157	0
$\overline{F}_s$	.02739	.02746	.02788	.02793	.02833
$\overline{F}_t$	.02891	.02899	.02788	.02950	.02833
Upper Wall					
$\overline{F}_p$	0	.00152	0	.00157	0
$\overline{F}_s$	.02793	.02735	.02787	.02794	.02818
$\overline{F}_t$	.02793	.02887	.02787	.02951	.02818
Total					
C_f	.00565	.00575	.00554	.00586	.00562
ratio	1.0199	1.0380	1	1.0440	1

However, a significant increase of pressure loss was also not observed. Overall the contribution from the shear stresses is marginally decreasing by the shallow dimples but the effect on the drag resistance is overcompensated by the newly appearing pressure force contribution. This outcome is consistent with an experimental investigation by Zhao et al. (2004) which for a hydraulically smooth channel also observed deviations of the friction coefficient with and without dimples within the margins of the measurement uncertainties. Concerning prospect applications of dimpled surfaces in engineering, it maybe assumed from the results reported that it is feasible to achieve an augmentation of heat transfer by shallow dimples without any additional pressure losses typically encountered for deep dimples.

ACKNOWLEDGMENTS

This work was supported by the *Deutsche Forschungsgemeinschaft* under contract number BR 1847/9. The computations were carried out on the NEC SX-8 machine at HLRS Stuttgart, which is gratefully acknowledged.

*

REFERENCES

Alekseev, V.V., Gachechiladze, I.A, Kiknadze, G.I. Oleinikov, V.G., 1998, "Tornado-like Energy Transfer on Three-Dimensional Concavities of Reliefs-Structure of Self-Organizing Flow, their Visualisation, and Surface Streamlining Mechanisms", *Transactions of the 2nd Russian Nat. Conf. of Heat Transfer*, vol. **6**, Heat Transfer Intensification Radiation and Complex Heat Transfer, Publishing House of Moscow Energy Inst. (MEI), Moscow, pp. 33–42.

Breuer, M., Rodi, W., 1996, "Large-Eddy Simulation of Complex Turbulent Flows of Practical Interest", In E. H. Hirschel, editor, *Flow Simulation with High-Performance Computers II*, vol. **52**, pp. 258–274. Vieweg Verlag, Braunschweig.

Breuer, M., 1998, "Large-Eddy Simulation of the Sub-Critical Flow Past a Circular Cylinder: Numerical and Modeling Aspects", *Int. J. for Num. Methods in Fluids*, vol. **28**, pp. 1281–1302.

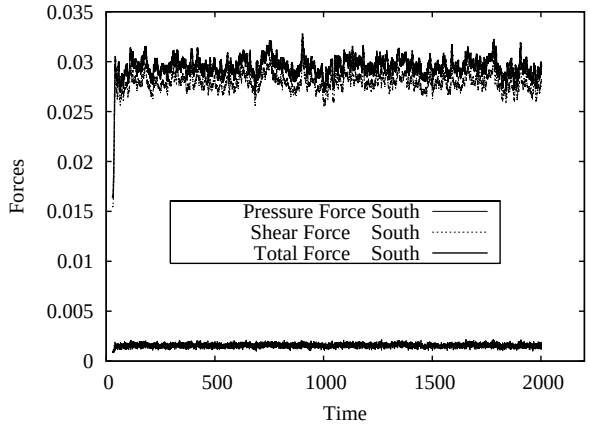

(a) **Forces at lower wall with dimples**

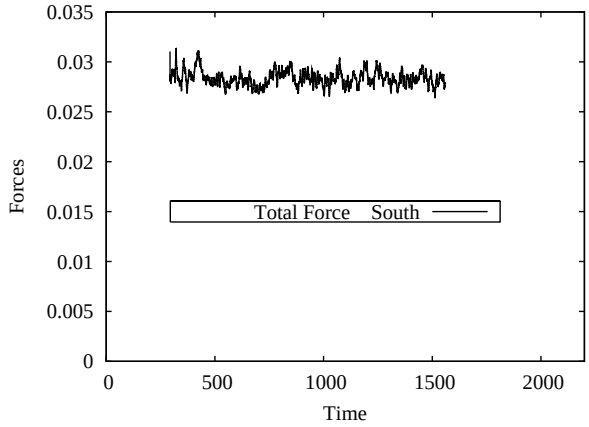

(b) **Forces at lower wall without dimples**

Figure 11: Time history of forces at the lower wall for case **B** and case **R**, fine grid simulation, $Re = 10,935$.

Breuer, M., 2002, "Direkte Numerische Simulation und Large-Eddy Simulation turbulenter Strömungen auf Hochleistungsrechnern", Habilitationsschrift, Univ. Erlangen-Nürnberg, *Berichte aus der Strömungstechnik*, ISBN: 3–8265–9958–6.

Bui, Trong T., Oates, David L., Gonsalez Jose C., 2000, "Design and Evaulation of a New Boundary-Layer Rake for Flight Testing", NASA/TM-2000-209014.

Burgess, N.K., Oliveira, M.M., Ligrani, P.M., 2003, "Nusselt Number Behavior on Deep Dimpled Surfaces Within a Channel", *J. Heat Transfer*, vol. **125**, pp. 11–18.

Dean, R.B., 1978, "Reynolds Number Dependence of Skin Friction and Other Bulk Flow Variables in Two-Dimensional Rectangular Duct Flow", *J. Fluids Engineering*, vol. **100**, pp. 215–223.

Moser, R.D., Kim, J., Mansour, N.N., 1999, "Direct Numerical Simulation of Turbulent Channel Flow up to Re_τ=590", *Phys. of Fluids A*, vol. **11** (4), pp. 943–945.

Zhao, J.B., Chew, Y.T, Khoo. B.C., 2004, "Experimental Studies on Hydrodynamic Resistance and Flow Pattern of a Narrow Flow Channel with Dimples on the Wall", Proc. ASME Int. Mech. Eng. Congress and Exhibition, Nov. 13–20, 2004, Anaheim, CA, USA, IMECE2004–59506.